

# Asymptotic solutions for a continuum model of a DC gas discharge in cavities with different geometry

L. Córdova-Castillo, J. M. Olvera-Orozco and S. Cuevas

*Instituto Energías Renovables, Universidad Nacional Autónoma de México,  
Apartado Postal 34, 62580, Temixco, Morelos, México.*

A. Figueroa

*CONACYT-Centro de Investigación en Ciencias, Universidad Autónoma del Estado de Morelos,  
Av. Universidad 1001, Chamilpa, 62209, Cuernavaca, Morelos, México.  
e-mail: alfil@uaem.mx*

F. Vázquez

*Centro de Investigación en Ciencias, Universidad Autónoma del Estado de Morelos,  
Av. Universidad 1001, Chamilpa, 62209, Cuernavaca, Morelos, México.*

Received 14 November 2021; accepted 2 March 2022

Analytical solutions for a continuum model of a DC gas discharge were obtained by asymptotic approximations. The solutions are one-dimensional and stationary. Three different cavity configurations of electrode pairs were considered, namely, parallel flat plates, concentric cylinders and concentric spheres. The asymptotic approximations consider nonlinear effects that are present in the dynamics of the plasma which are neglected in most of analytical solutions found in the literature. The obtained solutions determine the distribution of positively and negatively charged particles, as well as the electric potential along the space domain. Analytical results agree quantitatively with results from a spectral numerical solution developed for validation purposes. Such agreement was possible in a regime where the rate of charged particle production was assumed to be very small. Finally the limits of this regime are reported.

*Keywords:* DC gas discharge; electric potential; Avogadro's number.

DOI: <https://doi.org/10.31349/RevMexFis.68.051502>

## 1. Introduction

Electric gas discharges are carried out in many applications of industry and science. Glow discharge plasmas are considered cold even when they reach a mean temperature of approximately 11,600 K. Many weakly ionized laboratory plasmas are classified as low temperature plasmas [1,2]. Some of the most well-known technological applications that use cold plasmas are fluorescent luminaries (neon, mercury, etc.). Another application of plasma technology can be found in food industry, where the sterilization processes of a wide variety of vegetables are plasma-based at low temperatures [3]. Plasma technology is also used to sterilize thermolabile equipment and laboratory instruments that are sensitive to humidity [4]. However, some developments are so far limited by the poor knowledge of some of the basic properties of plasma. The inherent non-linear dynamics of plasma makes it difficult to describe [5]. Currently, glow discharges in different types of gases, subject to stationary electric and magnetic fields and temperature conditions, are under theoretical and experimental investigation with the aim of determining the spatial distribution of all charged and uncharged particle involved.

There is no single way to approach plasma modelling. A plasma is a system containing a very large amount of particles, usually of the order of Avogadro's number, which makes the description of individual particles hopeless. A com-

mon theoretical tool for plasma characterization is the macroscopic (fluid) approximation, which is the easiest option for cold plasma modelling. Evidence suggests that most macroscopic mathematical models for cold plasmas can be derived by considering all the involved species as fluids. This is a reasonable assumption if we consider a pressure range within 0.5 to 5 Torr [6]. These approaches for plasmas are valid if, for instance, the driving frequency of a radio-frequency (RF) discharge and the discharge gap are much larger than the electron energy relaxation time (of the order of nano seconds) and the mean free path (of the order of tens of  $\mu\text{m}$ ), respectively, making the fluid model suitable to be used in this regime [7].

It is well known that all available computational methods allow to consider diverse phenomena as, for instance, particle collisions and interactions, excitation, and recombination. Additionally, the use of numerical tools enables a proper handling of non-linearities, resulting in a more complete characterization of plasma dynamics [1]. Nevertheless, the theoretical problem of predicting plasma physics is not only reduced to the use of numerical tools, but can be addressed via analytical methods, whose capability to represent the physics of cold plasmas is highly appreciated in literature. Analytical solutions for cold plasma models have a reputation for being too complicated, mainly due to cumbersome boundary conditions and non-linearities which lead to oversimplifications [8], that in most cases reduce the underlying problem to a

set of diffusion equations [9]. However, there are advantageous physical situations that can be genuinely described by specific analytical solutions that cover most of the phenomena associated with such special cases. The latter, motivates the proposal to study basic but interesting cases of plasma physics which could be analysed with analytical tools. In our case, we use an analytical method that can be applied to model a wide range of cold plasma problems, with its specific physical assumptions, while taking into account phenomena such as recombination, attachment, and ionization. The proposed solution approaches the non-linear mathematical nature of a glow discharge by asymptotic expansions, which not only involve particle interactions but the advantage of non-linear effects to study three different geometrical configurations of electrodes: a pair of flat plates, a pair of concentric cylinders, and a pair of concentric spheres. With most of the cold plasma reactors developed in complex geometries, we consider the effect of cavity geometry in the behaviour of cold plasmas. In fact, a simple pair of coaxial cylindrical electrodes are directly applicable to the treatment of superconductive cavities, supersonic nozzles and particle accelerators, processes which imply the removal of chemical impurities that lead to electric losses or unfavorable hydrodynamic turbulence [10]. In order to estimate the predictive capabilities of the analytical method, we compare the analytical solutions with numerical calculations obtained through a high-order spectral method based on Chebyshev polynomials.

## 2. Physical model

The glow discharge in an inert monatomic gas is modelled under electrostatic DC configuration for three different geometrical cavities depicted in Fig. 1. The cavities are designed in such a way that the bounding walls act as the driving and ground electrodes, so that an electric potential can be applied through the walls in order to ionize the gas bounded inside the cavities. The electric connections in Fig. 1 are regularly used

in sputtering applications, where a negative voltage is applied to the cathode while the anode is grounded, commonly referred as cathodic sputtering [11]. The chamber where a discharge is performed often plays the role of the anode, assuming a zero potential in its surface. The first configuration, (Fig. 1a), consists of two flat plate parallel electrodes, the second configuration, (Fig. 1b), consists of two concentric cylindrical electrodes, where the outer one is a hollow cylinder and the inner one is a solid cylindrical rod. The third configuration, (Fig. 1c), consists of two concentric spherical electrodes, where the outer one is a hollow sphere and the inner sphere is solid. Notice that in all three cases, the region where the gas is ionized corresponds to the gap going from  $a$  to  $b$ , which is the distance separating the electrodes.

Once a constant gas flow reaches a stationary distribution inside the space between the electrodes, the powered electrodes reach the breakdown potential to ionize the monatomic gas. We assume that the ionization is obtained by collisions of electrons with neutral gas atoms, reaching the removal of only one electron in each collision. The creation of negative ions is neglected since only positive ions and free electrons are considered in the plasma dynamics. We do not consider any applied or induced magnetic field, thus magnetohydrodynamic effects are safely neglected. The recombination rate is considered constant and its contribution to the overall process is considered to be negligible. Furthermore, it is assumed that positive ions generated from collisions exchange energy through elastic collisions, and therefore are assumed to be at the same temperature as neutral species. The ion mobility and diffusivity coefficients are considered constant. Finally, we consider that at the macroscopic scale, as well as, the electron's and ion's mean temperatures are constants, so bulk gas convective motion is negligible. Our main aim is to characterize the plasma, in terms of the electric potential, electric field and spatial density distributions of positive and negative charges for each analysed geometry. Taking into account all these assumptions, the mathematical model is presented in the next section.

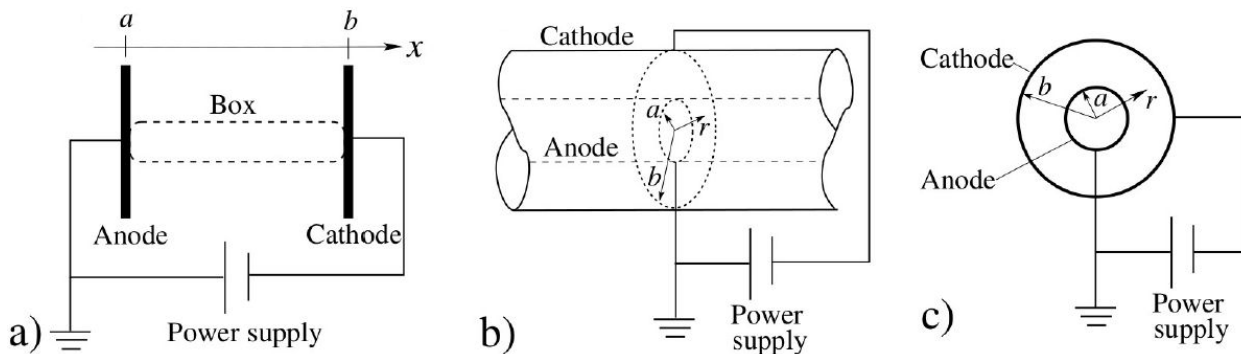


FIGURE 1. Sketch for the three arrays of cavities in which the glow discharge was modelled. a) Parallel flat electrodes. b) Concentric cylinders. c) Concentric spheres. For all the cases the non-powered anode was the grounded electrode.

### 3. Mathematical model

The cold plasma is modelled with the fluid approximation expressed in the following equations

$$\frac{\partial n_e}{\partial t} + \nabla \cdot \vec{J}_e = k_i, \quad (1)$$

$$\frac{\partial n_i}{\partial t} + \nabla \cdot \vec{J}_i = k_i, \quad (2)$$

$$\nabla^2 \varphi = \frac{e}{\epsilon} (n_e - n_i), \quad (3)$$

where Eqs. (1) and (2) are balance equations for electrons and ions densities  $n_e$  and  $n_i$ , while  $J_e$  and  $J_i$  are the electron and ion fluxes. Equation (3) is the Poisson's equation for the electric potential,  $\varphi$ , associated with the self-consistent electric field, resulting from the distributions  $n_e$  and  $n_i$  [6]. Here  $e$  is the electron's charge and  $\epsilon$  is the electric permittivity of the medium. The source term  $k_i$  considers the reaction rate (*i.e.* ionization only due to collisions of electrons with neutral gas atoms) occurring inside the chamber and is expressed as

$$k_i = k_{i0} N n_e \exp(-E_i/kT_e), \quad (4)$$

where  $k_{i0}$  is known as the pre-exponential factor of the reaction rate [12]. The Boltzmann constant, the electron temperature in K, the neutral particle concentration in the plasma, and the reaction activation energy are denoted by  $k$ ,  $T_e$ ,  $N$  and  $E_i$ , respectively. The particle fluxes of electrons and ions are given by

$$\vec{J}_e = -D_e \nabla n_e - \mu_e n_e \vec{E}, \quad (5)$$

$$\vec{J}_i = -D_i \nabla n_i + \mu_i n_i \vec{E}, \quad (6)$$

respectively, where  $\mu_i$  and  $\mu_e$  are the mobilities of ions and electrons, respectively, and  $D_i$  and  $D_e$  are the corresponding diffusion coefficients.  $\vec{E}$  is the total electric field which is calculated from

$$\vec{E} = -\nabla \varphi. \quad (7)$$

Equations (1)-(7) form a closed system which describes the glow discharge of cold plasmas that satisfies the boundary conditions described below.

#### 3.1. General boundary conditions

We make use of a very well established set of general boundary conditions but slightly modified in order to fit the restrictions of the analytical model. At the driving electrode (cathode), the electric potential satisfies the Dirichlet condition

$$\varphi = -V_c, \quad (8)$$

where  $V_c$  is the value of the applied electric potential at the cathode. For the electron density at the cathode we set

$$\begin{aligned} & \left( -D_e \nabla n_e - \mu_e n_e \vec{E} \right) \cdot \hat{n} \\ & = -\gamma \left( -D_i \nabla n_i + \mu_i n_i \vec{E} \right) \cdot \hat{n}, \end{aligned} \quad (9)$$

which includes the secondary emission phenomenon by setting the normal component of electron flux density to be proportional to the counterpart of positively charged ion flux modulated by an emission coefficient  $\gamma$ . We also assume that the cathode absorbs ions perfectly in the sense that any ion hitting the cathode surface captures a free electron emerging from it and is reflected into the core of the plasma as a neutral particle. Consequently, the ion density at the cathode satisfies

$$-D_i \nabla n_i \cdot \hat{n} = 0. \quad (10)$$

The boundary condition for the potential at the anode is depicted by

$$\varphi = V_A, \quad (11)$$

where  $V_A$  is the value of the applied potential at the anode, while the boundary condition for the electron density at the grounded electrode (anode) is

$$n_e = 0, \quad (12)$$

which implies zero concentration of electron density due to the assumption of infinitely fast recombination. Finally, since the anode does not emit (or absorb) ions, the net inward flux across its surface should vanish, *i.e.*,  $\vec{J}_i = 0$ , but for simplicity we shall again consider this boundary as a perfect absorber of ions, then ion density satisfies

$$-D_i \nabla n_i \cdot \hat{n} = 0. \quad (13)$$

Although conditions (8) - (13) would be the most appropriate, they will be modified properly due to specific limitations of the analytical method. Such modification that allows to faithfully compare our analytical and numerical solutions, will be explained in the results section. Additionally, an attempt to obtain a rough reproduction of computational results of glow discharges reported in literature is carried out.

#### 3.2. Dimensionless model

It is convenient to introduce the following dimensionless variables

$$\begin{aligned} n_e^* &= \frac{n_e}{n_0}, & n_i^* &= \frac{n_i}{n_0}, & \varphi^* &= \frac{\varphi}{V_0}, \\ t^* &= \frac{t}{\tau}, & \nabla^* &= \nabla L, & \vec{E}^* &= \frac{\vec{E}}{E_0}, \end{aligned} \quad (14)$$

where  $E_0 = V_0/L$ , the scale  $V_0$  being a characteristic value of potential related to the ionized gas (commonly the value of breakout potential). In our case,  $V_0 = V_c$  and  $L$  is a characteristic length scale imposed by the specific geometry of the cavity.  $n_0$  is a characteristic particle concentration scale, often considered as the neutral gas amount used in a discharge. The set of Eqs. (1) - (7) can be combined and reduced to just three equations by inserting the flux density Eqs. (5), (6) and (7) into Eqs. (1) and (2) respectively. Doing so, and introducing the dimensionless variables, we obtain a dimensionless

system of three transport equations for the densities of ions and electrons, and for the electric potential. Dropping the asterisk, the dimensionless system of equations for the cold plasma takes the following form

$$\xi \frac{\partial n_e}{\partial t} + P_e \nabla \varphi \cdot \nabla n_e = \nabla^2 n_e + D_a n_e + \Gamma P_e (n_i - n_e) n_e, \quad (15)$$

$$\xi \beta \frac{\partial n_i}{\partial t} - P_i \nabla \varphi \cdot \nabla n_i = \nabla^2 n_i + \beta D_a n_e - \Gamma P_i (n_i - n_e) n_i, \quad (16)$$

$$\nabla^2 \varphi = \Gamma (n_e - n_i), \quad (17)$$

where the dimensionless coefficients are defined as follows

$$P_e = \frac{\mu_e V_o}{D_e}, \quad P_i = \frac{\mu_i V_o}{D_i}, \quad \beta = \frac{D_e}{D_i}, \quad B = \frac{1}{k_B} T_0, \\ \xi = \frac{\nu L^2}{D_e}, \quad \Gamma = \frac{e n_o L^2}{V_o \epsilon}, \quad D_a = k_{i0} \frac{N L^2 e^{-BE_i}}{D_e},$$

where  $P_e$  and  $P_i$  are the Péclet numbers for electrons and ions, respectively,  $\Gamma$  a dimensionless value of the inverse characteristic potential and  $D_a$  is the Damkohler number that expresses the rate of ionization versus the diffusion of particles. Finally,  $\xi$  denotes the ratio of a characteristic frequency of the discharge and the diffusion of electrons. With the corresponding dimensionless notation, the set of boundary conditions at the cathode takes the final form

$$\varphi = -1, \quad (18)$$

$$(-\nabla n_e + P_e n_e \nabla \varphi) \cdot \hat{n} = -\frac{\gamma}{\beta} (-\nabla n_i - P_i n_i \nabla \varphi) \cdot \hat{n}, \quad (19)$$

$$-\nabla n_i \cdot \hat{n} = 0, \quad (20)$$

and at the anode

$$\varphi = 0, \quad (21)$$

$$n_e = 0, \quad (22)$$

$$-\nabla n_i \cdot \hat{n} = 0. \quad (23)$$

#### 4. Asymptotic solution

Assuming that the rate of ionization  $k_i$  inside the plasma is small, the Damkohler number can be considered as a small parameter, allowing the one-dimensional cold plasma model to be solved by asymptotic expansions for the three geometries shown in Fig. 1. The method of solution is described in this section with general assumptions. It is convenient to stress here that we try to model DC ionization assuming that the system remains in steady state and that the phenomenon is one-dimensional. We look for asymptotic solutions for  $n_e$ ,  $n_i$  and  $\varphi$  expressed as perturbation expansions in the small

parameter  $D_a$ , that is,

$$n_e = D_a n_e^{(1)} + D_a^2 n_e^{(2)} + D_a^3 n_e^{(3)} + \mathcal{O}(D_a^4), \quad (24)$$

$$n_i = D_a n_i^{(1)} + D_a^2 n_i^{(2)} + D_a^3 n_i^{(3)} + \mathcal{O}(D_a^4), \quad (25)$$

$$\varphi = D_a \varphi^{(1)} + D_a^2 \varphi^{(2)} + D_a^3 \varphi^{(3)} + \mathcal{O}(D_a^4), \quad (26)$$

where the superindex denotes the order of each term in the approximation. The symbol  $\mathcal{O}(D_a^4)$  represents all terms of order  $D_a^4$  and higher that are neglected in Eqs. (24)-(26). We now propose the final approximation by writing the term of ionization as follows:

$$D_a n_e = D_a \left( 1 + D_a^1 n_e^{(1)} + D_a^2 n_e^{(2)} + D_a^3 n_e^{(3)} + \mathcal{O}(D_a^4) \right). \quad (27)$$

By substitution of (24)-(27) into Eqs. (15)-(17) the solutions for  $n_e$ ,  $n_i$  and  $\varphi$  that satisfy boundary conditions (18)-(23) can be obtained to the considered order. The explicit analytic expression of the solutions for  $n_e$ ,  $n_i$  and  $\varphi$  for the flat parallel electrodes geometry are presented in the Appendix. Lastly, we note the approximate contribution of each order to the general solution. The first order terms proportional to  $\mathcal{O}(D_a)$  contributes 99.967 % of the solution. Terms of  $\mathcal{O}(D_a^2)$  contributes approximately 0.032 %, while the contribution of  $\mathcal{O}(D_a^3)$  is three orders of magnitude smaller. Even though the second and third order contributions become numerically insignificant to our analytical solution, there is justification to keep them. First of all, the first-order conditions seemed to be incomplete in mathematical terms. Furthermore, adding the  $\mathcal{O}(D_a^2)$  term, the solutions near the boundaries were qualitatively improved. The  $\mathcal{O}(D_a^3)$  term is comprised in our solution just for illustration purposes and due to the ease of its calculation.

#### 5. Numerical solution

A Chebyshev spectral collocation method (CSCM) was used to obtain a numerical solution for the cold plasma model defined by Eqs. (15)-(17). The details of CSCM can be found in the specialized literature [13-16]. Let us consider the Chebyshev approximation of  $n_e(x)$ ,  $n_i(x)$ ,  $\varphi(x)$  defined in a one dimensional rectilinear coordinate for  $x \in [-1, 1]$  as

$$n_e(x) = \sum_{k=0}^N \hat{u}_k^{(e)} T_k^{(e)}(x), \quad (28)$$

$$n_i(x) = \sum_{k=0}^N \hat{u}_k^{(i)} T_k^{(i)}(x), \quad (29)$$

$$\varphi(x) = \sum_{k=0}^N \hat{u}_k^{(\varphi)} T_k^{(\varphi)}(x), \quad (30)$$

where the upper index  $(e)$ ,  $(i)$  and  $(\varphi)$  stands for the Chebyshev polynomials and the coefficients for electron density, ion density and electric potential, respectively. The order of approximation is denoted by  $N$ . The differential equations are

satisfied at certain points called the Gauss-Lobatto collocation points, represented as

$$x = \cos\left(\frac{i\pi}{N}\right). \quad (31)$$

In the case of the cylindrical, spherical and even with rectilinear coordinates, we use a mapping of any arbitrary interval  $r \in [R_1, R_2]$  to standard interval  $x \in [-1, 1]$ , which is needed to fit the requirement of Chebyshev polynomials, that is,

$$r = \frac{(R_2 - R_1)x + R_2 + R_1}{2}. \quad (32)$$

Derivatives are thus treated as

$$\frac{\partial}{\partial r} = \frac{2}{R_2 - R_1} \frac{\partial}{\partial x} \quad \text{and} \quad \frac{\partial^2}{\partial r^2} = \left(\frac{2}{R_2 - R_1}\right)^2 \frac{\partial^2}{\partial x^2}. \quad (33)$$

## 6. Results

### 6.1. Linear regime

In this section, we present the results obtained from the mathematical model in the linear regime, where the dimensionless parameters  $P_e, P_i, \Gamma, \gamma$  and  $\beta$  take values less or equal to unity. Results of the analytical procedure are compared against results from the numerical method in Fig. 2. Since

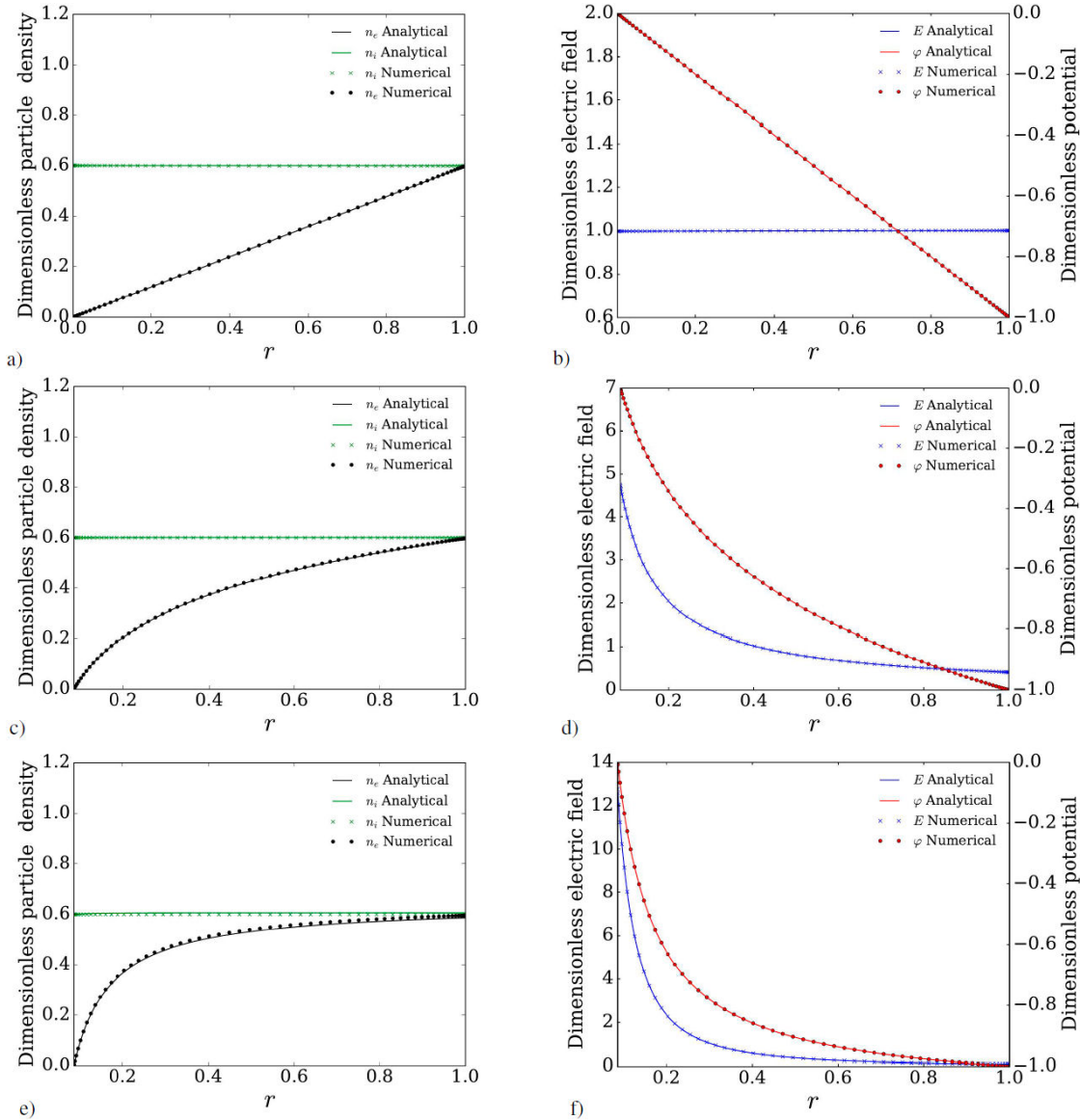


FIGURE 2. Electron density, ion density, potential and electric field profiles. Linear regime. First row: Parallel flat plates. Second row: Concentric cylinders. Third row: Concentric spheres. Continuous lines: Analytical model. Symbols: Numerical solutions.

analytically is not possible to consider Neumann boundary conditions on both boundaries, the boundary condition of ion density at the cathode (20) was replaced by the expression  $n_i = ni_c = 0.6$ . Such value is actually the one obtained in numerical calculations when we apply Neumann boundary conditions (20) and (23). The dimensionless parameters in this regime, used for the whole set of electrodes were:  $D_a = 3.3 \times 10^{-4}$ ,  $\Gamma = 10^{-2}$ ,  $\beta = 10^{-2}$ ,  $\gamma = 10^{-2}$ ,  $P_e = 10^{-2}$ ,  $P_i = 1$  and the values for the potential were  $\varphi = -1$  and  $\varphi = 0$ , at the cathode and the anode, respectively. These parameters fulfill the requirement of a linear regime. Finally, the parallel set of flat electrodes were positioned at  $a = 0$  and  $b = 1$ . In turn, both the cylindrical and spherical electrodes were positioned at  $a = 0.085$  and  $b = 1$ .

Figure 2 shows an excellent comparison between the analytical and numerical results for the three geometrical configurations of electrodes. At this point we can show that our numerical and analytical tools are mathematically consistent with each other. Therefore, we can emphasize the distinct distribution of particles and fields within each pair electrodes. This is mainly due to the difference in surface area of each pair of electrodes. Evidently, if the surface electric charge is measured in an arbitrary position at the same distance from the anode or the cathode in each system, different values will be obtained. Therefore, it appears that the accumulation or absence of charge in these surfaces is abruptly modified from one geometry to the other. This is clearly illustrated in the behavior of the electric field and the electric potential near the anode, namely, in the Figs. 2b, 2d and 2f. Since all results were obtained with the same values of the transport coefficients, it can be stated that geometry takes a relevant role (perhaps the most important) in the distribution of potential, electric field, and of course particles. This is confirmed by the agreement of both methods of solution. The availability of the analytical solutions in the linear regime allows for the validation of numerical models of cold plasmas.

## 6.2. Non-linear regime

In this section we present the comparison of asymptotic and numerical results of the model formulated by Eqs. (15)-(17) for a cold plasma in the non-linear regime, which inherently implies large values of  $P_e \sim 10^2$  and  $P_i \sim 10^3$  using common discharge conditions in Argon. These conditions imply that drift process becomes relevant, and diffusion, although not negligible, is not the only process involved. There is also a relevant fact about the value of  $\beta \sim 10^4$  which implies that electron diffusion is many orders of magnitude larger than ion diffusion. Lastly, the parameter  $\Gamma$  indicates the magnitude of the inverse potential. It is important to highlight that the requirements that makes the analytical solution mathematically valid are not fulfilled in this regime, but for the sake of comparison, they are also obtained to show their limitations. Finally, it turns out that the trends of the analytical solutions are very similar to those obtained with numerical calculations.

In Fig. 3a), we observe that ion and electron distribu-

tions resemble bell-shaped curves. In addition, the peak of ion and electron density are approximately 1.62 and 1.49, respectively, for asymptotic results, while for numerical results, these peaks were found at 1.38 and 1.35, respectively. We can observe that in the non-linear regime, only a qualitative agreement between the analytical and the numerical solutions is obtained. These theoretical results present qualitative similarities with solutions obtained in the literature with different numerical methods [17-19]. Notice that the ion densities at the powered electrode ( $r=1$ ) present different boundary conditions in the numerical solution with respect to the analytical one. This is due to the fact that in the numerical solution we used Neumann conditions (20) and (23), being easy to implement in both electrodes, whereas analytically this is not easily accomplished, and  $n_i = 0$  was imposed instead of (20) at the cathode for the analytical solution.

It is important to remark that the parameters were different for the numerical and the analytical results. The parameters used in the numerical calculations were  $D_a = 5.5 \times 10^{-5}$ ,  $\Gamma = 488.9$ ,  $\beta = 10^4$ ,  $\gamma = 0.046$ ,  $P_e = 0.9$ ,  $P_i = 900$ . The parameters used in the analytical calculations were  $D_a = 5.5 \times 10^{-4}$ ,  $\Gamma = 200$ ,  $\beta = 10^4$ ,  $\gamma = 0.046$ ,  $P_e = 25$ ,  $P_i = 0.15$ . The choice of the latter dimensionless values in the analytical solutions is due to the fact that they yield results qualitatively similar to the numerical ones. For the other set of electrodes such values were obtained by trial and error considering them as an estimate of those used in the numerical solutions. Figure 3b) shows the potential and electric field distributions for the flat plate electrodes configuration. The electric charge of the plasma is predominantly positive in most of the gap between electrodes. The potential satisfies the boundary conditions imposed, which are  $\varphi = -1$  at the cathode and  $\varphi = 0$  at the grounded electrode.

The stationary distributions of ions and electrons for the case of cylindrical electrodes are shown in Fig. 3c) along with the electric field and electric potential distributions in Fig. 3d). The analytical solution shown in Fig. 3c) qualitatively reproduces many features of the numerical solution except for  $n_i$ . The value of the parameters used in the numerical calculations were  $D_a = 60 \times 10^{-6}$ ,  $\Gamma = 1$ ,  $\beta = 10^3$ ,  $\gamma = 0.022$ ,  $P_e = 0.5$ ,  $P_i = 40$ . In turn, the parameters used in the analytical calculations were  $D_a = 60 \times 10^{-6}$ ,  $\Gamma = 0.01$ ,  $\beta = 10^3$ ,  $\gamma = 0.022$ ,  $P_e = 0.5$ ,  $P_i = 40$ . The values of the parameters used for the numerical solution were estimated from those used in the literature. Therefore, distributions of particle density and electric fields are comparable to results reported experimentally and numerically [20]. It is worth noting that the behaviour of our system was disturbed with a low level of drift of electrons, leaving diffusion to become the most relevant transport mechanism. In the case of ion transport, drift is the most important phenomenon in the core of the plasma. Finally, in Fig. 3d) we can observe a similar slow decay in the potential as well as in the electric field along the space between electrodes, but much sharper in the latter.

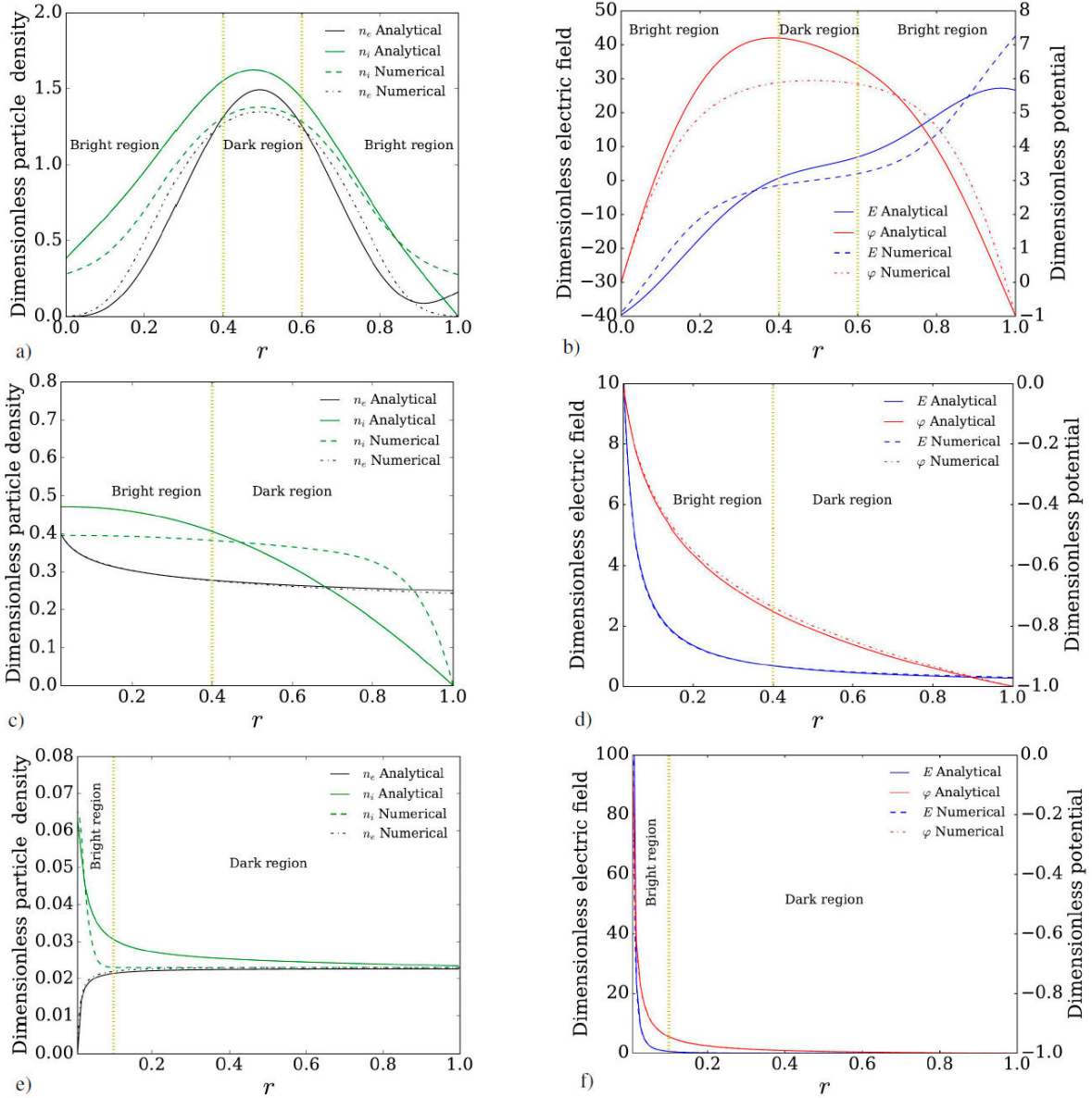


FIGURE 3. Electron density, ion density, potential and electric field profiles. Non-linear regime. First row: Parallel flat plates. Second row: Concentric cylinders. Third row: Concentric spheres. Continuous lines: Analytical model. Symbols: Numerical solutions.

Figure 3e) shows ion and electron distributions for the concentric spheres case, where a predominantly positive plasma can be observed near the inner electrode. The complete set of boundary conditions are (19)-(23) with a modification for the ion density at the anode in Eq. (23), used for both the analytical and the numerical solutions, namely,  $J_i = J_A$  at  $r = 0.006$ . Results and boundary conditions presented here are an attempt to qualitatively reproduce results reported in a specific work [21]. Here,  $J_A$  is a specific value of electric current which could be measured in the anode, but we chose  $J_A = -10$ . However, for both numerical and analytical solutions, the ion density takes a positive value in the cathode at  $r = 1$  as a result of an imposed Dirichlet condition, which implies the modification of condition (20) into  $n_i = 0.024$ . The parameters used in the

numerical model were  $D_a = 40 \times 10^{-5}$ ,  $\Gamma = 1$ ,  $\beta = 10^2$ ,  $\gamma = 0.01$ ,  $P_e = 0.09$ ,  $P_i = 10$  and for the analytical solutions,  $D_a = 40 \times 10^{-5}$ ,  $\Gamma = 0.1$ ,  $\beta = 10$ ,  $\gamma = 0.001$ ,  $P_e = 0.001$ ,  $P_i = 96$ . In this specific set of electrodes we observe a difference between the analytical and numerical results for the ion density. However, as seen in Fig. 3f), there exists a case of the distribution of the electric field and potential where the profiles of the numerical and analytical solution are very similar.

The results presented in Fig. 3e) indicate that the case of two concentric spherical electrodes is mainly characterized by a considerable increase of the concentration of charged particles in the anode region, especially of the positive species. While the glow discharge in flat geometry Fig. 3b) is characterized by a smooth behaviour of potential

and electric field in most of the discharge gap, an abrupt drop in potential in the glow discharge is observed in the spherical and cylindrical geometries.

Experimental observations of the glow discharges between parallel electrodes [22] and cylindrical electrodes (hollow cathode) [23] show the generation of luminous and dark regions within the plasma. In order to contrast the experimental observations with our results, the yellow dotted vertical lines in Fig. 3 delimit the bright and dark regions within the plasma. In the parallel electrodes configuration, first row in Fig. 3), the electric field magnitude is low between  $r = 0.4$  and  $r = 0.6$ , which denotes a dark region (or Faraday dark space). Outside the latter region, the electric field magnitude is increased, which promotes two bright regions denoted as anode and cathode glow. For the cylindrical electrodes, second row in Fig. 3, we can only identify two regions, the anode glow close to the inner electrode due to the increase in particle density and electric field magnitude, and the dark one which covers most of the system. A similar distribution of the bright and the dark regions can be appreciated for the concentric spheres case, third row in Fig. 3, however in this case the anode glow is shorter than the previous case (concentric cylinders) due to the abrupt decay of the electric field in the  $r$ -direction. We must note that, the physics of a DC glow discharge is more complex than our theoretical approach which only reproduces some qualitative aspects of real glow discharges because of the strongly restrictive assumptions. However, these asymptotic solutions represent a simple useful tool to understand some basic aspects of DC glow discharges.

## 7. Concluding Remarks

Analytical and numerical solutions for a non-linear mathematical model of a cold plasma were found for different electrode configurations. A glow discharge was achieved by ion-

ization of an inert gas with an applied electric field between the gap of three different configurations of electrode pairs. Analyzed configurations correspond to parallel plate, concentric cylindrical and concentric spherical electrodes. With the aim of determining electron and ion densities as well as potential an electric field distributions, asymptotic expansions were implemented to solve the plasma model analytically with power series in terms of the Damkohler number, that were truncated up to third order to make the problem manageable.

Regarding the comparison with the available numerical results, the analytical solutions are strongly limited by boundary conditions and the asymptotic approximation. Nevertheless, we developed a numerical tool based on a spectral method to solve the complete set of equations of the cold plasma model. By maintaining the dimensionless parameters within a given range, it was possible to exactly match the numerical and the analytical results in the three electrode configurations. Thus, the theoretical scope of the present work is limited by the values with which the dimensionless parameters can achieve coinciding numerical and analytical results.

We found that our analytical and numerical results agree qualitatively in the non-linear regime as compared with results found in literature. Nonetheless, given to the scarcity of exact solutions in the literature our asymptotic solution in the linear regime is useful for the validation of numerical models for cold plasma with the specific assumptions mentioned in this work.

## Appendix A.

Asymptotic solutions up to second order for the flat parallel electrodes geometry for electron, ion and potential

$$n_e^{(1)}(x) = \frac{(a-x)(a+x-2)}{2}, \quad (\text{A.1})$$

$$\begin{aligned} n_e^{(2)}(x) = & -\frac{1}{144(a-1)\beta}a-x(a-1\beta^2(P_e x(-2x^4+12x^3-18x^2-3x+9)+15\gamma P_i+a^3(P_e(5x^2+42x-27)-150\gamma P_i) \\ & +a^5(2P_e-15\gamma P_i)+a^4(P_e(3-13x)+75\gamma P_i)-a(P_e(2x^4+12x^3-63x^2+30x+9)+75\gamma P_i) \\ & +a^2(P_e(10x^3-45x^2-18x+33)+150\gamma P_i))\Gamma+6ni_c P_i \gamma(24V_c+(a-1)^2(5-10a+5a^2-12ni_c)\Gamma) \\ & +\beta(-48+72\gamma P_i V_c+12\Gamma P_e x^4-2\Gamma P_e x^5+15\gamma \Gamma P_i-66\gamma \Gamma ni_c P_i+a^5\Gamma(P_e(13x-1)-90\gamma P_i) \\ & -9P_e x(\Gamma(4ni_c-1)+8V_c)-6x^3(3\Gamma(ni_c+1)P_e+1)+3x^2(\Gamma(20ni_c-1)P_e+8P_e V_c+8)+a^6(15\gamma \Gamma P_i-2\Gamma P_e) \\ & +a^4(\Gamma P_e(6ni_c-5(x^2+11x-6))+3\gamma \Gamma(75-22ni_c)P_i-30)+a^2(-6P_e(\Gamma(8ni_c-7)+8V_c) \\ & +6x^2(\Gamma(ni_c-18)P_e+1)+6x(\Gamma(13ni_c+2)P_e+13)+9\gamma P_i(\Gamma(25-44ni_c)+8V_c)+2\Gamma P_e x^4+22\Gamma P_e x^3-264) \\ & -2a^3(-3(\Gamma(ni_c-10)P_e+2\gamma \Gamma(22ni_c-25)P_i+25)+15x(\Gamma(ni_c-2)P_e+1)+5\Gamma P_e x^3-25\Gamma P_e x^2) \\ & +a(192-14\Gamma P_e x^4+2\Gamma P_e x^5-6P_i \gamma(24V_c+\Gamma(15-44ni_c))+9P_e(\Gamma(4ni_c-1)+8V_c) \\ & -6x^2(11\Gamma(ni_c-1)P_e+5)+3x(-\Gamma(4ni_c+13)P_e+8P_e V_c-16)+6x^3(P_e(\Gamma+3\Gamma ni_c)+1))), \end{aligned} \quad (\text{A.2})$$

$$n_i^{(1)}(x) = \frac{\beta(a-x)(a+x-2)}{2} + ni_c, \quad (\text{A.3})$$

$$\begin{aligned}
n_i^{(2)}(x) = & -\frac{1}{144(a-1)}a - x(-6(a-1)\Gamma ni_c P_i(a+x-2)(5a^2 - 10a - 12ni_c - x^2 + 2x + 4) + a - 1P_i(-15 + 13a^5 \\
& + 13a^4(x-6) - 9x + 3x^2 + 18x^3 - a^3(-5x^2 - 42x + 177) + a^2(-10x^3 + 45x^2 + 18x - 183) + a(2x^4 + 12x^3 - 63x^2 \\
& + 30x + 84) + 2x^5 + 12x^4)\beta^2\Gamma - \beta(-48 + 72P_i V_c + 15\Gamma P_i + 13a^6\Gamma P_i - 84\Gamma ni_c P_i + 13a^5\Gamma P_i(x-7) + 12\Gamma P_i x^4 \\
& - 2\Gamma P_i x^5 - 9P_i x(\Gamma(4ni_c - 1) + 8V_c) - 6x^3(\Gamma(4ni_c + 3)P_i + 1) + 3x^2(\Gamma(28ni_c - 1)P_i + 8P_i V_c + 8) - 5a^4(\Gamma P_i(12ni_c \\
& + x^2 + 11x - 51) + 6) - 10a^3(-6\Gamma(5ni_c - 6)P_i + x(6\Gamma(ni_c - 1)P_i + 3) + \Gamma P_i x^3 - 5\Gamma P_i x^2 - 15) + a(192 - 72P_i V_c \\
& - 99\Gamma P_i + 372\Gamma ni_c P_i + 3x(-\Gamma(20ni_c + 13)P_i + 8P_i V_c - 16) + 6x^3(P_i(\Gamma + 4\Gamma ni_c) + 1) - 6x^2(\Gamma(16ni_c - 11)P_i + 5) \\
& + 2\Gamma P_i x^5 - 14\Gamma P_i x^4) + a^2(22\Gamma P_i x^3 + 3(\Gamma(89 - 176ni_c)P_i + 8P_i V_c - 88) \\
& + 6x^2(2\Gamma(ni_c - 9)P_i + 1) + 6x(2P_i(\Gamma + 13\Gamma ni_c) + 13) + 2\Gamma P_i x^4)), \tag{A.4}
\end{aligned}$$

$$\varphi^{(1)}(x) = \frac{(a-x)((a-1)\Gamma(x-1)(5a^2(\beta-1) - a(\beta-1)(x+9) + 12ni_c - (\beta-1)((x-3)x-3)) + 24V_c)}{24(a-1)}, \tag{A.5}$$

$$\begin{aligned}
\varphi^{(2)}(x) = & -\frac{1}{20160(a-1)\beta}a - xx - 1\Gamma(a-1P_i(385 + 716a^6 + 385x + 35x^2 - 70x^3 - 49x^4 + 35x^5 - 5x^6 - 2a^5(97x + 2051) + a^4(-194x^2 \\
& + 1358x + 9576) + 4a^3(4x^3 + 182x^2 - 861x - 2905) + a^2(51x^4 - 252x^3 - 714x^2 + 3920x + 7735) - a(5x^5 + 77x^4 - 406x^3 - 70x^2 \\
& + 1995x + 2695))\beta^3\Gamma - 140ni_c P_i(-1 + 2a - x)\gamma(a-1)^2\Gamma(5a^2 - 10a - 12ni_c + 5) + 24V_c + \beta^2(-35\Gamma x^5(P_e - P_i) + 5\Gamma x^6(P_e - P_i) \\
& + 2a^6(2P_e(39x - 67) + P_i(2409 + (97 - 175\gamma)x - 2275\gamma))\Gamma) + 4a^7\Gamma(4P_e + (175\gamma - 179)P_i) - 7x^2(-8\Gamma ni_c P_i + 5\Gamma P_e - 5\Gamma P_i \\
& + 96P_i V_c - 20) + 14x^3(34\Gamma ni_c P_i + 5\Gamma P_e - 5\Gamma P_i + 12P_i V_c + 10) + 7x^4(-\Gamma(16ni_c + 7)P_i + 7\Gamma P_e - 4) + 2a^5(\Gamma P_i(6300\gamma + 1694ni_c \\
& + 97x^2 + 1050\gamma x - 776x - 6839) + \Gamma P_e(-97x^2 - 274x + 539) + 854) + 7x(144P_i V_c + \Gamma P_i(-50\gamma - 272ni_c + 55) - 5(\Gamma P_e + 28)) \\
& - 7(\Gamma P_i(50\gamma + 272ni_c - 55) + 5(\Gamma P_e + 28) - 144P_i V_c) + a^2(-128\Gamma x^4(P_e - P_i) + 5\Gamma x^5(P_i - P_e) + 14x^3(\Gamma(2ni_c - 47)P_i + 47\Gamma P_e \\
& + 2) + 28x^2(28\Gamma(3ni_c - 1)P_i + 28\Gamma P_e + 39) - 14(5\Gamma P_i(135\gamma + 380ni_c - 149) + 70\Gamma P_e - 312P_i V_c + 970) + 7x(-5\Gamma P_i(150\gamma + 276ni_c \\
& - 169) - 95\Gamma P_e + 24P_i V_c - 660)) + 2a^4(461\Gamma x^2(P_e - P_i) + 8\Gamma x^3(P_e - P_i) + 7x(\Gamma P_i(-375\gamma - 58ni_c + 343) + 32\Gamma P_e - 28) \\
& - 7(\Gamma P_i(1375\gamma + 1152ni_c - 1514) + 139\Gamma P_e + 582)) + a(40\Gamma x^5(P_e - P_i) + 5\Gamma x^6(P_i - P_e) + 28x^4(\Gamma(4ni_c - 1)P_i + \Gamma P_e + 1) \\
& - 28x^3(6 + 17\Gamma P_e + (-17 + 18ni_c)P_i\Gamma) - 28x(\Gamma P_i(-75\gamma - 268ni_c + 85) - 10(\Gamma P_e + 13) + 24P_i V_c) + 56(\Gamma P_i(50\gamma + 204ni_c - 55) \\
& + 5(\Gamma P_e + 21) - 72P_i V_c) + 7x^2(24P_i V_c + \Gamma(5 - 228ni_c)P_i - 5(\Gamma P_e + 24))) + a^3(-268\Gamma x^3(P_e - P_i) + 51\Gamma x^4(P_e - P_i) \\
& - 14x^2(\Gamma(58ni_c - 103)P_i + 103\Gamma P_e + 28) + 28x(\Gamma P_i(250\gamma + 174ni_c - 263) + 13\Gamma P_e + 84) + 7(-216P_i V_c + 5\Gamma P_i(500\gamma + 852ni_c \\
& - 553) + 5(53\Gamma P_e + 432))) - \beta(-35\Gamma P_e x^5 + 5\Gamma P_e x^6 + 4a^7\Gamma(4P_e + 175\gamma P_i) + 2a^6\Gamma(2P_e(39x - 67) - 175\gamma P_i(x + 13)) \\
& - 14x^3(10 + 12P_e V_c + \Gamma(24ni_c - 5)P_e - 10\Gamma ni_c P_i) + 7x^4(\Gamma(12ni_c + 7)P_e - 4\Gamma ni_c P_i + 4) + 7(10\Gamma P_i(-5\gamma + 36ni_c^2 + 2(11\gamma - 7)ni_c) \\
& + \Gamma(12ni_c - 5)P_e + 96P_e V_c - 240\gamma P_i V_c + 140) + 7x(10\Gamma P_i(-5\gamma + 36ni_c^2 + 2(11\gamma - 7)ni_c) + \Gamma(12ni_c - 5)P_e + 96P_e V_c \\
& - 240\gamma P_i V_c + 140) + 7x^2(-20(6\Gamma ni_c^2 P_i - \Gamma ni_c P_i + 1) + \Gamma(12ni_c - 5)P_e + 96P_e V_c) - 2a^5(14((110\gamma - 61)\Gamma ni_c P_i - 75\gamma\Gamma P_i(x + 6) \\
& + 61) + \Gamma P_e(97x^2 + 274x - 539)) + 2a^4(461\Gamma P_e x^2 + 8\Gamma P_e x^3 - 7x(-28 + 2\Gamma(15ni_c - 16)P_e + 2(14 - 55\gamma)\Gamma ni_c P_i + 375\gamma\Gamma P_i) \\
& + 7(\Gamma(30ni_c - 139)P_e + 6(165\gamma - 97)\Gamma ni_c P_i - 1375\gamma\Gamma P_i + 582)) + a^3(-268\Gamma P_e x^3 + 51\Gamma P_e x^4 + 14x^2(\Gamma(30ni_c - 103)P_e - 28\Gamma ni_c P_i \\
& + 28) + 28x(\Gamma(30ni_c + 13)P_e + 4(21 - 55\gamma)\Gamma ni_c P_i + 250\gamma\Gamma P_i - 84) - 7(20\Gamma P_i(-125\gamma + 30ni_c^2 + 4(44\gamma - 27)ni_c) + 5\Gamma(36ni_c \\
& - 53)P_e + 264P_e V_c - 480\gamma P_i V_c + 2160)) - a(-40\Gamma P_e x^5 + 5\Gamma P_e x^6 - 28x^3(\Gamma(12ni_c - 17)P_e - 6\Gamma ni_c P_i + 6) + 28x^4(\Gamma(3ni_c - 1)P_e \\
& - \Gamma ni_c P_i + 1) + 56(105 + 48P_e V_c - 120\gamma P_i V_c + \Gamma(9ni_c - 5)P_e + 5\Gamma P_i(-10\gamma + 36ni_c^2 + 3(11\gamma - 7)ni_c)) + 28x(5\Gamma P_i(-15\gamma + 24ni_c^2 \\
& + (44\gamma - 26)ni_c) + 2\Gamma(9ni_c - 5)P_e + 96P_e V_c - 120\gamma P_i V_c + 130) + 7x^2(24P_e V_c + \Gamma(5 - 108ni_c)P_e - 120(\Gamma ni_c^2 P_i - \Gamma ni_c P_i + 1))) \\
& + a^2(-128\Gamma P_e x^4 - 5\Gamma P_e x^5 - 28x^2(\Gamma(45ni_c - 28)P_e - 39\Gamma ni_c P_i + 39) + 14x^3(2\Gamma ni_c P_i + 47\Gamma P_e - 2) + 14(5\Gamma P_i(-135\gamma + 168ni_c^2 \\
& + 2(154\gamma - 97)ni_c) + 10\Gamma(9ni_c - 7)P_e + 288P_e V_c - 600\gamma P_i V_c + 970) + 7x(P_e(216V_c - 95\Gamma) + 30(22 - 8\gamma P_i V_c + P_i(4ni_c^2 \\
& - 25\gamma + 22(2\gamma - 1)ni_c\Gamma))))). \tag{A.6}
\end{aligned}$$

## Acknowledgments

This research was supported by CONACYT, Mexico, under project 258623. A. Figueroa thanks the “Investigadoras e Investigadores por México” program from CONACYT.

- 
1. F. Lei, X. Li, D. Liu, Y. Liu, and S. Zhang, *AIP Advances* **9** (2019) 085228 <https://doi.org/10.1063/1.5118911>.
  2. Y. Liu, D. Liu, J. Zhang, B. Sun, A. Yang, and M. G. Kong, *Physics of Plasmas* **27** (2020) 043512, <https://doi.org/10.1063/1.5145033>.
  3. Y. Liang *et al.*, *Environmental science & technology* **46** (2012) 3360, <https://doi.org/10.1021/es203770q>.
  4. L. A. Feldman and H. Hui, *Method of protecting and sterilizing aluminum surfaces on medical instruments*, (1997), uS Patent 5,658,529.
  5. H. Shi, Y. Wang, and D. Wang, *Physics of Plasmas* **15** (2008) 122306, <https://doi.org/10.1063/1.3033754>.
  6. D. B. Graves and K. F. Jensen, *IEEE Transactions on Plasma Science* **14** (1986) 78.
  7. Y. P. Raizer and J. E. Allen, *Gas discharge physics*, **Vol. 2** (Springer Berlin, 1997) pp. 8-20.
  8. S. Gao, S. Chen, Z. Ji, W. Tian, and J. Chen, *Advances in Mathematical Physics* **2017** (2017) 1, <https://doi.org/10.1155/2017/9193149>.
  9. M. V. Straaten, R. Gijbels, and A. Vertes, *Analytical Chemistry* **64** (1992) 1855, <https://doi.org/10.1021/ac00041a021>.
  10. J. Upadhyay, J. Peshl, S. Popović, A.-M. Valente-Feliciano, and L. Vušković, *AIP Advances* **8** (2018) 085008, <https://doi.org/10.1063/1.5045692>.
  11. J. T. Gudmundsson, *Plasma Sources Science and Technology* **29** (2020) 113001 <https://doi.org/10.1088/1361-6595/abb7bd>.
  12. J. J. Shang, *Aerospace* **5** (2018) 2, <https://doi.org/10.3390/aerospace5010002>.
  13. L. N. Trefethen, (1996).
  14. R. Peyret, *Spectral methods for incompressible viscous flow*, **Vol. 148** (Springer Science & Business Media, 2002) pp. 40-80.
  15. C. Canuto *et al.*, *Spectral methods in fluid dynamics* (Springer Science and Business Media, 2012).
  16. J. P. Boyd, *Chebyshev and Fourier spectral methods* (Courier Corporation, 2001) pp. 19-57.
  17. A. Figueroa *et al.*, *Plasma Science and Technology-Progress in Physical States and Chemical Reactions* (InTech, 2016) <https://doi.org/10.5772/62096>.
  18. Y. hung Lin and R. A. Adomaitis, *Journal of Computational Physics* **171** (2001) 731, <https://doi.org/10.1006/jcph.2001.6808>.
  19. A. Bouchikhi and A. Hamid (2008).
  20. S. Gao, J. Feng, W. Li, and J. Cai, *The European Physical Journal Applied Physics* **88** (2019) 30801, <https://doi.org/10.1051/epjap/2019190224>.
  21. Y. Lelyukh and V. Zhovtyansky, *Ukrainian Journal of Physics* **53** (2008) 497.
  22. J. T. Gudmundsson and A. Hecimovic, *Plasma Sources Science and Technology* **26** (2017) 123001, <https://doi.org/10.1088/1361-6595/aa940d>.
  23. M. Nurujjaman, R. Narayanan, and A. N. Sekar Iyengar, *Chaos: An Interdisciplinary Journal of Nonlinear Science* **17** (2007) 043121, <https://doi.org/10.1063/1.2815818>.